Immune Netw. 2021 Dec;21(6):e44
https://doi.org/10.4110/in.2021.21.e44
pISSN 1598-2629·eISSN 2092-6685

IMMUNE NETWORK

Original Article

Induction of Peptide-specific CTL Activity and Inhibition of Tumor Growth Following Immunization with Nanoparticles Coated with Tumor Peptide-MHC-I Complexes

Sang-Hyun Kim [1], **Ha-Eun Park** [1], **Seong-Un Jeong** [1], **Jun-Hyeok Moon** [1], **Young-Ran Lee** [2], **Jeong-Ki Kim** [3], **Hyunseok Kong** [4], **Chan-Su Park** [5,*], **Chong-Kil Lee** [1,*]

[1]Department of Pharmaceutics, College of Pharmacy, Chungbuk National University, Cheongju 28644, Korea
[2]Center for Convergence Bioceramic Materials, Korea Institute of Ceramic Engineering and Technology, Cheongju 28160, Korea
[3]Department of Pharmacy, Korea University College of Pharmacy, Sejong 30019, Korea
[4]Department of Animal Biotechnology and Resource, Sahmyook University, Seoul 01795, Korea
[5]Department of Pathology, The Johns Hopkins University School of Medicine, Baltimore, MD 21205, USA

Received: Nov 17, 2021
Revised: Dec 13, 2021
Accepted: Dec 15, 2021

***Correspondence to**
Chong-Kil Lee
Department of Pharmaceutics, College of Pharmacy, Chungbuk National University, 1 Chungdae-ro, Seowon-gu, Cheongju 28644, Korea.
E-mail: cklee@chungbuk.ac.kr

Chan-Su Park
Department of Pathology, The Johns Hopkins University School of Medicine, Baltimore, MD 21205, USA.
E-mail: cpark52@jhmi.edu

ORCID iDs
Sang-Hyun Kim
https://orcid.org/0000-0002-7360-0491
Ha-Eun Park
https://orcid.org/0000-0002-9046-7637
Seong-Un Jeong
https://orcid.org/0000-0001-7654-8521
Jun-Hyeok Moon
https://orcid.org/0000-0002-5159-0923

ABSTRACT

Tumor peptides associated with MHC class I molecules or their synthetic variants have attracted great attention for their potential use as vaccines to induce tumor-specific CTLs. However, the outcome of clinical trials of peptide-based tumor vaccines has been disappointing. There are various reasons for this lack of success, such as difficulties in delivering the peptides specifically to professional Ag-presenting cells, short peptide half-life *in vivo*, and limited peptide immunogenicity. We report here a novel peptide vaccination strategy that efficiently induces peptide-specific CTLs. Nanoparticles (NPs) were fabricated from a biodegradable polymer, poly(D,L-lactic-co-glycolic acid), attached to H-2K^b molecules, and then the natural peptide epitopes associated with the H-2K^b molecules were exchanged with a model tumor peptide, SIINFEKL ($OVA_{257-268}$). These NPs were efficiently phagocytosed by immature dendritic cells (DCs), inducing DC maturation and activation. In addition, the DCs that phagocytosed SIINFEKL-pulsed NPs potently activated SIINFEKL-H-2K^b complex-specific CD8$^+$ T cells via cross-presentation of SIINFEKL. *In vivo* studies showed that intravenous administration of SIINFEKL-pulsed NPs effectively generated SIINFEKL-specific CD8$^+$ T cells in both normal and tumor-bearing mice. Furthermore, intravenous administration of SIINFEKL-pulsed NPs into EG7.OVA tumor-bearing mice almost completely inhibited the tumor growth. These results demonstrate that vaccination with polymeric NPs coated with tumor peptide-MHC-I complexes is a novel strategy for efficient induction of tumor-specific CTLs.

Keywords: Polymeric nanoparticle; Tumor peptide; Peptide-MHC-I complex; Tumor vaccine; Cytotoxic T lymphocyte; Anti-tumor activity

Young-Ran Lee
https://orcid.org/0000-0001-8696-5513
Jeong-Ki Kim
https://orcid.org/0000-0003-1520-1377
Hyunseok Kong
https://orcid.org/0000-0002-4880-6340
Chan-Su Park
https://orcid.org/0000-0003-4968-8304
Chong-Kil Lee
https://orcid.org/0000-0001-9070-341X

Conflict of Interest
The authors declare no potential conflicts of interest.

Abbreviations
APC, Ag-presenting cell; BMDC, bone marrow-derived DC; DC, dendritic cell; EDC, 1-ethyl-3-(3-dimethylaminopropyl) carbodiimide hydrochloride; NP, nanoparticle; NP-Ab, Ab-conjugated NP; NP-Ab-Kb, NP-Ab attached with H-2Kb; NP[FITC], NP containing FITC; NHS, N-hydroxysuccinimide; PEMA, poly(ethylene/maleic anhydride); PLGA, poly(D, L-lactic-co-glycolic acid); PVA, polyvinyl alcohol; W/O, water-in-oil.

Author Contributions
Conceptualization: Lee YR, Kim JK, Kong H, Park CS, Lee CK; Data curation: Lee YR; Investigation: Kim SH, Park HE, Jeong SU, Moon JH, Park CS; Writing - original draft: Kim SH; Writing - review & editing: Park CS, Lee CK.

INTRODUCTION

Many tumors express peptide antigens, which are typically 8 to 10 amino acids long and are presented in association with MHC-I molecules (1). Mounting evidence indicates that the induction of tumor peptide-specific CTLs is a critical factor for successful anti-tumor immunotherapy (2). Tumor peptides have been classified into two categories: tumor-associated Ags, which are over-expressed in tumors compared to normal tissues, and tumor-specific Ags, which are exclusively expressed in tumors and not in non-malignant tissues (3-6).

The tumor peptides associated with MHC-I molecules or their synthetic variants have attracted great attention for their potential use in inducing tumor-specific CTLs (7-10). However, the results of clinical trials using peptide vaccines have been disappointing (11). Currently, more than 66 clinical trials have been registered in ClinicalTrials.gov, yet no peptide-based vaccines have been approved by the Food and Drug Administration of the United States. One of the major limitations of peptide vaccines is that the peptide itself has limited immunogenicity and generates weak cellular responses (12). To increase the immunogenicity of peptide vaccines, strategies in which the peptides are combined with adjuvants, such as TLR agonist and anti-CD40 mAb, have been developed with some success (8,12-15). Yet another critical limitation is that upon *in vivo* administration, the peptides may indiscriminately bind to MHC-I molecules expressed on the surface of numerous types of cells apart from the professional Ag-presenting cells (APCs). Activation of naïve $CD8^+$ T cells requires at least two distinct signals delivered from professional APCs. The first signal is generated by the antigenic peptide-MHC-I complexes that interact with TCRs, and the second, by costimulatory molecules such as CD80 and CD86 that interact with CD28 on T cells (16-20). Interaction between peptide-MHC-I complexes and TCR in the absence of the second signal induces T cell anergy or apoptosis, rather than stimulation (18). Thus, the binding of *in vivo*-administered peptides to MHC-I molecules expressed in non-APCs would critically limit the effectiveness of the peptide vaccine.

We report here a novel peptide vaccination strategy to efficiently induce peptide-specific CTLs *in vivo*. The essence of this vaccine strategy is the fabrication of biodegradable nanoparticles (NPs) coated with MHC-I-binding peptide epitopes. The peptides attached to the NPs are delivered specifically to phagocytic cells, including DCs, which are cross-presented to $CD8^+$ T cells to efficiently induce peptide-specific CTLs. We believe this peptide vaccination strategy involving NPs could be a novel means to overcome the several limitations encountered with free-form peptide vaccination, such as the binding of the peptides to MHC-I molecules expressed in non-professional APCs, poor immunogenicity, rapid degradation of peptides by tissue and serum peptidases, and poor DC activation.

MATERIALS AND METHODS

Animals

Female C57BL/6 mice (8–12 weeks old) were purchased from KosaBio Inc. (Seongnam, Korea). All experimental procedures involving animals were approved by the Animal Care Committee of Chungbuk National University (CBNUA-1490-21-02), and performed in accordance with the guidelines and regulations.

Preparation of carboxlyated NPs

Carboxylated NPs were prepared using a solvent evaporation method. Briefly, 8 ml of 1% poly(ethylene/maleic anhydride) (PEMA; Polysciences Inc., Warrington, PA, USA) aqueous solution was mixed with 4 ml of 5% poly(D, L-lactic-co-glycolic acid) (PLGA; Evonik Industries, Essen, Germany) dissolved in ethyl acetate. The mixture was then homogenized at 14,000 rpm for 4 min to form a water-in-oil (W/O) emulsion. To solidify the NPs, the W/O emulsion was transferred to a beaker containing 0.2% PEMA and 0.1% polyvinyl alcohol (PVA; Sigma-Aldrich, St. Louis, MS, USA) and then stirred for approximately 18–24 h. The resulting NPs were centrifuged at 3,500×*g* for 20 min at 4°C, washed twice with distilled water, and resuspended in 10 ml of sterile distilled water. Fluorescence-labeled NPs were prepared by adding FITC (Sigma-Aldrich) to the ethyl acetate.

Isolation of membrane proteins containing H-2K^b

Membrane proteins containing H-2K^b (K^b) were isolated from an EG7.OVA tumor mass. Briefly, 1 g of EG7.OVA tumor mass was dissociated with 10 ml of extraction buffer containing 0.15 M NaCl, 0.05 M sodium phosphate buffer (pH 7.0), and 1X protease inhibitor cocktail (Sigma-Aldrich) using gentlMACS dissociator (Miltenyi Biotec, Bergisch Gladbach, Germany). After removing cell debris and lipids, the supernatant was ultra-centrifuged at 80,000 × *g* for 45 min at 4°C using Ultracentrifuge (Beckman Coulter, Brea, CA, USA). The pellet was homogenized in 0.5 ml of extraction buffer using Tissue Grinder (SHS-30E; SciLab, Seoul, Korea). The homogenate was then mixed with 0.5 ml of solubilization buffer containing 2% n-dodecyl β-D-maltoside and 0.4% 3-[(3-cholamidopropyl)dimethyl ammonio]-1-propanesulfonate hydrate (Sigma-Aldrich) in extraction buffer and solubilized for 90 min at 4°C. The supernatant containing membrane proteins was obtained by centrifugation at 17,000 rpm for 30 min at 4°C. The amount of isolated membrane proteins was determined using a microbicinchoninic acid assay kit (ThermoFisher Scientific, Rockford, IL, USA).

Preparation of anti-mouse K^b mAb-conjugated NPs and tumor-derived K^b-attached NPs

Anti-K^b mAbs were conjugated to the carboxylated NPs by using the 1-ethyl-3-(3-dimethylaminopropyl)carbodiimide hydrochloride (EDC; ThermoFisher Scientific)/N-hydroxysuccinimide (NHS; Sigma-Aldrich) coupling method. Briefly, 10 mg of carboxylated NPs was resuspended in 1.2 ml of 50 mM activation buffer (4-morpholineethanesulfonic acid buffer, pH 6.0, Sigma-Aldrich) and treated with 4 μL of 300 mM EDC and 8 μL of 300 mM NHS for 1 h at 24–26°C. The EDC-activated NPs were washed twice with 50 mM activation buffer and then resuspended in 1 ml of 50 mM activation buffer containing 600 μg/ml anti-mouse K^b mAbs (Clone Y-3; BioXcell, Lebanon, NH, USA) for 18 h at room temperature. The Ab-conjugated NPs were treated with 30 μL of ethanolamine (Sigma-Aldrich) for 30 min to quench the reaction of free EDC-activated carboxyl residues and washed twice with PBS. To attach K^b, Ab-conjugated NPs were incubated with tumor-derived membrane proteins for 24 h at 4°C. The K^b-attached NPs were washed twice with PBS and resuspended in 1 ml of PBS.

Characterization of carboxylated NPs and K^b-attached NPs

The mean size and ζ-potential of carboxylated NPs were measured using a particle size analyzer (ELS-Z, Otsuka, Japan). The morphology of carboxylated NPs was visualized by scanning electron microscopy (LEO-1530, Carl Zeiss, Germany). The particle number of NPs was counted using qNano Gold (IZON Science, Christchurch, New Zealand). K^b-attached NPs were stained with anti-mIgG (BioLegend, San Diego, CA, USA) and anti-K^b (BD Biosciences,

San Jose, CA, USA) mAbs for 30 min and analyzed using flow cytometry (FACS Canto II, BD Biosciences). Flow cytometry data was analyzed using FlowJo software (TreeStar, Ashland, OR, USA).

Preparation of bone marrow-derived DC (BMDC)

DCs were generated as described previously (21). Briefly, the bone marrow cells obtained from mouse femurs were cultured in 6-well plates (5×10^6 cells/well) in a culture medium with 40 ng/ml GM-CSF and 20 ng/ml IL-4 (Creagene, Seongnam, Korea). On days 3 and 4, non-adherent cells were removed by gently shaking the dish, and the medium was replaced. The cells, referred to as immature BMDC, were harvested on day-6 by gentle pipetting and used for further experiments.

Phagocytosis analysis

The FITC-labeled NPs (2×10^9 particles/well) were added to a mouse DC cell line, DC2.4 cells (2×10^6 cells/well), in 6-well plate. After 2 h, the non-phagocytosed NPs were removed by washing twice with pre-warmed PBS. The cells were harvested, fixed with 1% paraformaldehyde in PBS, and analyzed using flow cytometry. For confocal analysis, 50 nM LysoTracker Red DND-99 (Thermo Fisher Scientific) together with the FITC-labeled NPs (5×10^8 particles/well) were added to the DC2.4 cells (5×10^5 cells/well) in 6-well plate. After 2 h, the non-phagocytosed NPs were removed by washing twice with pre-warmed PBS. The cells were fixed with 4% paraformaldehyde in PBS, mounted with Antifade Mounting Medium with DAPI (Vector Laboratories Inc., Burlingame, CA, USA), and visualized using a confocal microscope (K1-fluo; Nanoscope Systems Inc., Daejeon, Korea).

Phenotype analysis

Immature BMDCs were seeded in 24-well plates (1×10^6 cells/well) and stimulated with 100 ng/ml LPS or treated with the NPs (1×10^9 particles/well) for 24 h. BMDCs were harvested and stained with mAbs to detect the mouse cell surface markers (CD11c, H-2K^b, I-A^b, CD80, and CD86) and isotype-matched control Abs (BD Biosciences), as described previously (21).

Cytokine production analysis

Immature BMDCs were seeded in 24-well plates (1×10^6 cells/well) and stimulated with 100 ng/ml LPS or treated with the NPs (1×10^9 particles/well). After 24 h, the culture supernatants were harvested, and the amounts of IL-1β, IL-6, and TNF-α were measured using commercial ELISA kits (BD Biosciences).

Peptide exchange reaction in K^b-attached NPs

To exchange the native peptide with SIINFEKL (Peptron, Daejeon, Korea), 5 mg of K^b-attached NPs was incubated with 20 μM or 100 μM SIINFEKL for 18 h at 37°C, washed twice with PBS, and resuspended in 0.5 ml of PBS. The level of SIINFEKL bound to the K^b-attached NPs was analyzed with mAbs recognizing the SIINFEKL-K^b complex (25-D1.16; BioLegend).

MHC-I-restricted cross-presentation assay

DC2.4 cells (1×10^5 cells/well) were incubated with the NPs (1×10^8 particles/well) in 96-well plate for 2 h, washed with pre-warmed PBS, fixed with 1% paraformaldehyde, and washed again with PBS. The SIINFEKL-specific CD8$^+$ T cell stimulatory capacity of the DC2.4 cells was measured using SIINFEKL-specific CD8$^+$ T cell hybridoma CD8OVA cells (2×10^5 cells/well), which recognize SIINFEKL-K^b complexes and secrete IL-2 in response, as previously described (22).

https://doi.org/10.4110/in.2021.21.e44

In vivo generation of SIINFEKL-specific CD8$^+$ T cells

C57BL/6 mice were intravenously immunized with PBS or the NPs (1×10^9 particles/mouse) on days 0 and 7. On days 5 and 12, whole blood samples were collected from the facial vein, stained with T-Select H-2K^b OVA Tetramer (MBL, Tokyo, Japan) and mouse CD8α mAb (Clone KT15; BioLegend), and analyzed using flow cytometry, according to the manufacturer's instructions.

In vivo SIINFEKL-specific CTL assay

C57BL/6 mice were intravenously immunized with PBS or the NPs (1×10^9 particles/mouse) on days 0 and 7. On day 14, SIINFEKL-specific CTL activity was assessed by an *in vivo* CTL assay, as described previously (21). Target cells were syngeneic splenocytes pulsed with 1 μM SIINFEKL and labeled with 25 μM CFSE. Syngeneic splenocytes labeled with 5 μM CFSE without SIINFEKL pulsing were used as control target cells. The specific killing of SIINFEKL-pulsed target cells was determined by analyzing spleen cells and lymph node cells isolated from each recipient mouse via flow cytometry.

Anti-tumor activity

The right flank of each C57BL/6 mouse was shaved and subcutaneously inoculated with EG7.OVA cells (3×10^5 cells/mouse). Mice were then intravenously administered the indicated NP preparations (1×10^9 particles/mouse) on days 2, 9, and 16. The tumor was measured every 2 days using calipers, and the tumor volume was calculated using the following formula: tumor volume [mm^3] = 0.52 × (long diameter [mm]) × (short diameter [mm])^2.

Statistical analysis

A two-tailed paired Student's *t*-test was performed for single comparisons of two groups after an evaluation for normality. One-way or two-way ANOVA with a *post-hoc* Tukey's test were performed to determine significant differences among multiple groups; $p \leq 0.05$ was considered statistically significant.

RESULTS

Fabrication and characterization of K^b-attached NPs

Carboxylated NPs were fabricated with PLGA and PEMA using the W/O emulsion solvent evaporation method. The mean size of the carboxylated NPs was 767.0±79.9 nm (**Fig. 1A**), which falls within the optimal size range for DC uptake (23,24). The average polydispersity index and ζ-potential of the carboxylated NPs were 0.258±0.021 and −38.61±0.35 mV, respectively (**Fig. 1A**, **Supplementary Table 1**). The carboxylated NPs had a spherical shape with a relatively homogeneous size distribution, as shown by scanning microphotography (**Fig. 1B**).

The carboxylated NPs (bare NPs) were then covalently coupled with anti-K^b mAbs (isotype mIgG2b) by carbodiimide conjugation. The Ab-conjugated NPs (NP-Ab) were incubated with solubilized membrane proteins isolated from the EG7.OVA tumor mass (H-2^b) to prepare K^b-attached NPs (NP-Ab-K^b). Attachment of Ab and K^b molecules to NPs was confirmed by flow cytometry after staining with PE-labeled anti-mIgG and FITC-labeled anti-K^b mAb. The NPs were successfully coated with anti-K^b (98.2%) and K^b (83.9%) (**Fig. 1C**). An increase in the average size (767.0±79.9 to 903.1±32.2 nm) and a decrease in the ζ-potential (−38.61±0.35 to −18.68±3.64 mV) indicated that Ab and K^b were immobilized on the NP surface in expense of carboxyl residues (**Supplementary Table 1**).

https://doi.org/10.4110/in.2021.21.e44

NP-Ab-K^b in PBS was stable for at least 9 days, when stored at 4°C, with respect to average particle size, ζ-potential, and the attachment of both Ab and K^b molecules (**Fig. 1D, E, and F**). The number of K^b molecules immobilized per NP was estimated to be 1.56×10^4, as determined using NP-Ab-K^d which were prepared with the same methods used for the fabrication of NP-Ab-K^b (**Supplementary Table 2**).

DCs efficiently phagocytose NP-Ab-K^b

To examine the efficiency of NP-Ab-K^b uptake by DCs, we prepared carboxylated NPs containing FITC (NP[FITC]) and then generated NP[FITC]-Ab and NP[FITC]-Ab-K^b. Each type of NP was added to cultures of DC2.4 cells for 2 h and washed with PBS, and the degree of phagocytosis was analyzed using flow cytometry. DC2.4 cells phagocytosed NP[FITC]-Ab and NP[FITC]-Ab-K^b much more efficiently compared to NP[FITC] phagocytosis (**Fig. 2A**). The MFI values of DC2.4 cells treated with NP[FITC]-Ab and NP[FITC]-Ab-K^b were 15.2-fold and 11.6-fold higher, respectively, than that of DC2.4 cells treated with NP[FITC] control (**Fig. 2B**). It is reasonable to speculate that the increased phagocytosis of NP[FITC]-Ab and NP[FITC]-Ab-K^b is due to the opsonization effect of the Ab. The NP[FITC]-Ab was fabricated so that the Fc fragment of Ab attached to the NP, leaving the Ag-binding site exposed outside (25). However, some of the Abs could be conjugated via the Ag-binding site, leaving the Fc region exposed outside. The relative decrease in the phagocytosis of NP[FITC]-Ab-K^b compared to that of NP[FITC]-Ab might be explained by the steric hindrance of the Fc by the K^b attached nearby.

Internalization of the NPs was confirmed by confocal imaging. The colocalization of NPs and lysosomes appeared as yellow fluorescence upon overlaying green fluorescent NPs and red fluorescent lysosomes (**Fig. 2C**).

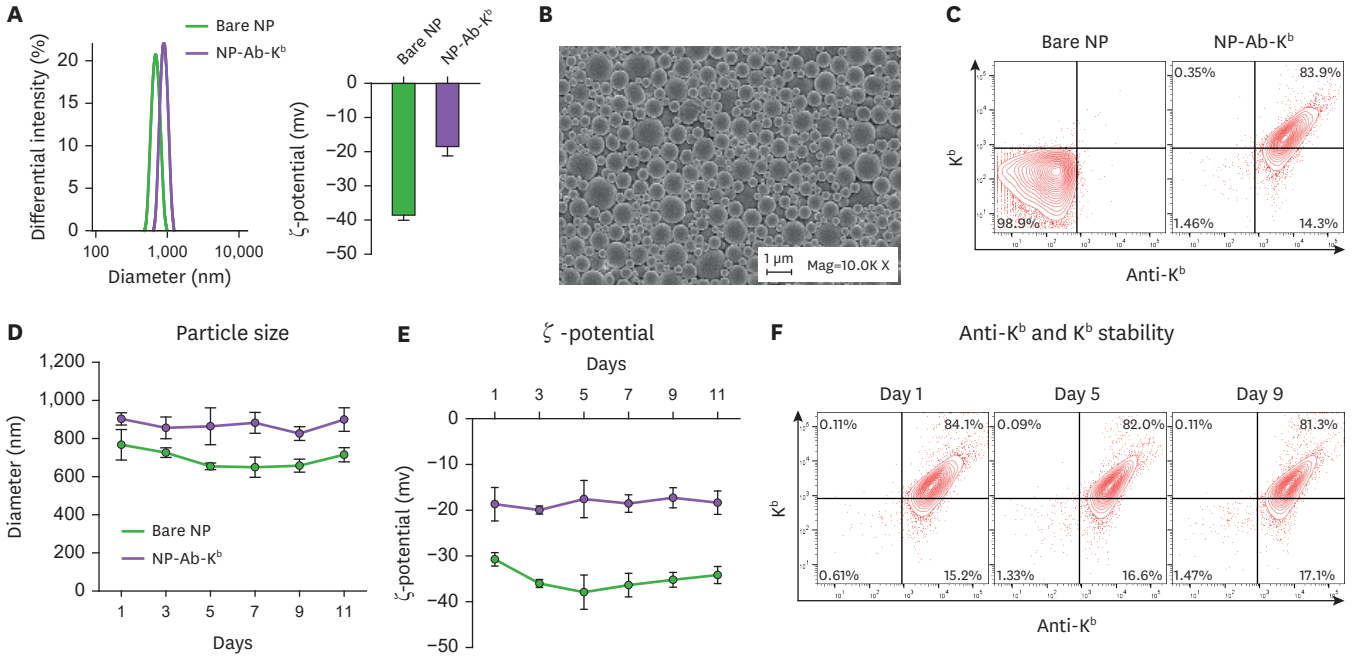

Figure 1. Characterization of NP-Ab-K^b. (A) The average size and ζ-potential of bare NPs, as determined by a particle size analyzer, were 767.0±79.9 nm and -38.61±0.35 mV, respectively. (B) Scanning electron microscopy image showing bare NPs with spherical shapes and a relatively homogeneous size distribution. (C) Attachment of Ab and K^b molecules to NPs was confirmed by flow cytometry after staining with fluorochrome-labeled anti-mIgG and anti-K^b. Stability of NP-Ab-K^b with respect to: (D) average particle size, (E) ζ-potential, and (F) the attachment of both Ab and K^b molecules, for at least 9 days. In E and F, the data are presented as mean ± SD of three independent experiments.

https://doi.org/10.4110/in.2021.21.e44

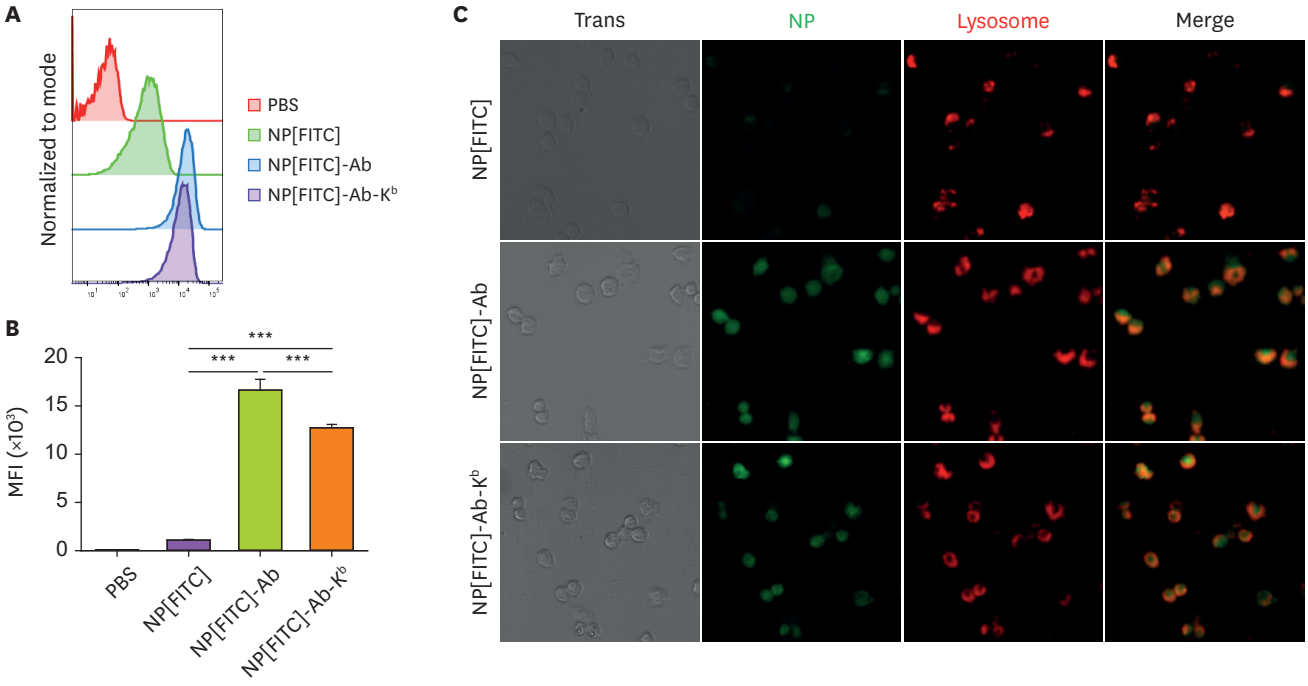

Figure 2. DC2.4 cells efficiently phagocytose NP[FITC]-Ab-K^b. (A) DC2.4 cells were treated with NP[FITC], NP[FITC]-Ab, or NP[FITC]-Ab-K^b, and the degree of phagocytosis was analyzed by flow cytometry. (B) Mean fluorescence intensities of DC2.4 cells treated with NP[FITC], NP[FITC]-Ab, or NP[FITC]-Ab-K^b. The data are presented as the mean ± SD of three independent experiments.(C) DC2.4 cells (5×10^5 cells/well) were treated with NP[FITC], NP[FITC]-Ab, or NP[FITC]-Ab-K^b in the presence of LysoTracker Red DND-99 for 2 h, and internalization of the NPs was determined via confocal imaging. Significant differences between groups were evaluated by one-way ANOVA with a *post-hoc* Tukey's test.
***p<0.001.

Phagocytosis of NP-Ab-K^b induces maturation and activation of immature DCs

To investigate the effects of NP-Ab-K^b on the maturation and cytokine production of DCs, immature BMDCs were exposed to NP-Ab-K^b for 24 h. Control DCs were treated with PBS, bare NP, or NP-Ab, or matured with LPS. Phenotypic analysis of the DCs showed that NP-Ab-K^b–treated BMDCs expressed much higher levels of CD80, CD86, and MHC-II (I-A^b) molecules, all of which are associated with Ag-specific T cell priming, than PBS-treated immature BMDCs (**Fig. 3A**). The phenotypic maturation-inducing activity appeared to be stronger in the order of bare NP, NP-Ab-K^b, NP-Ab, and LPS. BMDCs treated with NP-Ab-K^b produced much higher amounts of the pro-inflammatory cytokines IL-1β, IL-6, and TNF-α than PBS-treated immature BMDCs (**Fig. 3B**). The cytokine-inducing activity of NP-Ab-K^b was higher than that of bare NP, but significantly lower than that of NP-Ab. These results align with the NP phagocytic activity of the DCs (**Fig. 2**). As expected, NP-Ab-K^b, which was fabricated with PLGA and PEMA, did not exert cytotoxic effects on DCs. Conversely, NP-Ab-K^b induced DC proliferation when added to the cultures for 24 h (**Supplementary Fig. 1**).

SIINFEKL-pulsed NP-Ab-K^b efficiently induces MHC-I-restricted cross-presentation of SIINFEKL in DCs

The natural peptide epitopes associated within the K^b molecules of NP-Ab-K^b were exchanged with a model tumor-specific peptide, SIINFEKL. NP-Ab-K^b was incubated with 0, 20, or 100 μM of SIINFEKL for 2 to 18 h at 37°C, and then the relative degree of the SIINFEKL exchange reaction was assessed using an mAb (Clone 25-D1.16) that recognizes the SIINFEKL-K^b complexes. The SIINFEKL exchange reaction was maximal when NP-Ab-K^b was incubated with 100 μM SIINFEKL for 18 h (**Fig. 4**).

https://doi.org/10.4110/in.2021.21.e44

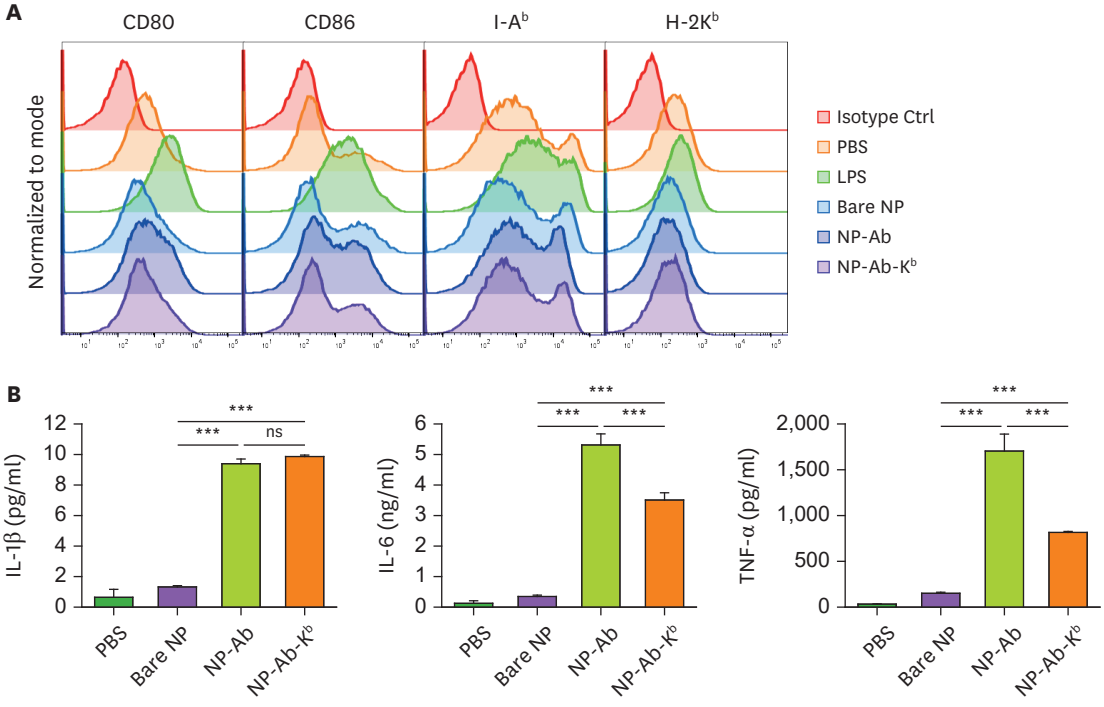

Figure 3. Phagocytosis of NP-Ab-K^b induces activation in immature DCs. (A) Immature BMDCs were cultured with LPS (100 ng/ml), bare NP, NP-Ab, or NP-Ab-K^b (1×10^9 particles/well) for 24 h and stained for CD11c, H-2K^b, I-A^b, CD80, and CD86. CD11c$^+$ cells were gated and analyzed for the expression of cell surface molecules. The data show representative histograms of three independent experiments. (B) Immature BMDCs were cultured with PBS, bare NP, NP-Ab, or NP-Ab-K^b for 24 h, and the cytokine levels in the culture supernatant were determined by ELISA. As a control, immature BMDCs were treated with LPS, and shown to induce the production of 254.9 pg/ml IL-1β, 15.9 ng/ml IL-6, and 14.3 ng/ml TNF-α. The data are presented as the mean ± SD of three independent experiments. ***p<0.001; ns, no significant difference.

The cross-priming capacity of the DCs treated with SIINFEKL-pulsed NP-Ab-K^b was investigated using an MHC-I-restricted cross-presentation assay. DC2.4 cells were incubated with SIINFEKL-pulsed NP-Ab-K^b for 2 h, washed and fixed, and then co-cultured with SIINFEKL-specific CD8$^+$ T cell hybridoma, CD8OVA cells, which recognize SIINFEKL-K^b complexes and secrete IL-2. DCs treated with SIINFEKL-pulsed NP-Ab-K^b potently activated CD8OVA cells, and the activation-inducing activity was dependent on the SIINFEKL concentration used for the peptide exchange reaction (**Fig. 5A**). DCs treated with SIINFEKL-unpulsed NP-Ab-K^b also activated CD8OVA cells, although the potency of activation was extremely low compared to that of SIINFEKL-pulsed NP-Ab-K^b (**Fig. 5B**). It is noteworthy that K^b molecules were isolated from EG7.OVA tumor tissue; thus, some of the K^b molecules were naturally complexed with SIINFEKL.

SIINFEKL-pulsed NP-Ab-K^b induces SIINFEKL-specific CTLs in normal and tumor-bearing mice

Specific CTL-inducing activity of SIINFEKL-pulsed NP-Ab-K^b was first examined in normal mice. The optimal particle number of SIINFEKL-pulsed NP-Ab-K^b for inducing SIINFEKL-specific CTLs was 1×10^9 particles/mouse (**Supplementary Fig. 2**). Accordingly, mice were i.v. injected with SIINFEKL-pulsed NP-Ab-K^b (1×10^9 particles/mouse) twice, with an interval of 7 days. Control mice were i.v. injected with PBS or bare NP. Five days after the last immunization, peripheral blood was collected from each mouse by cheek bleeding, and SIINFEKL-specific CTLs were analyzed using SIINFEKL-loaded K^b tetramers. Immunization of mice with SIINFEKL-pulsed NP-Ab-K^b potently induced SIINFEKL-specific CTLs (**Fig. 6A**). The percentage of SIINFEKL-specific CTLs among CD8$^+$ T cells reached 1.8% when 20 μM SIINFEKL-pulsed

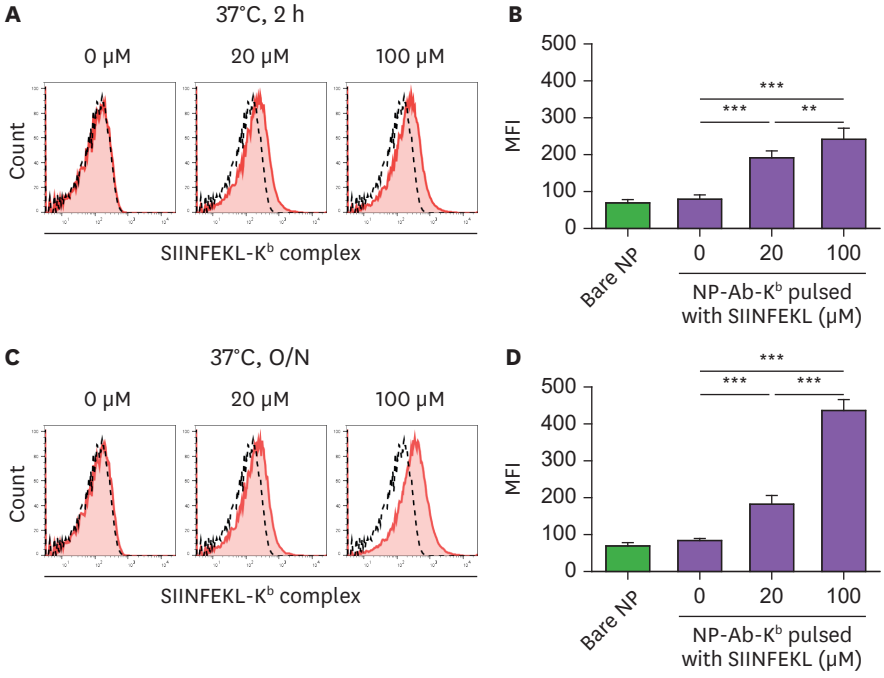

Figure 4. Effect of SIINFEKL concentration and reaction time on peptide exchange reaction in NP-Ab-K^b. (A) NP-Ab-K^b was incubated with 0, 20, or 100 μM SIINFEKL for 2 h at 37°C. SIINFEKL-pulsed NP-Ab-K^b was stained using an mAb (Clone 25-D1.16) for the SIINFEKL-K^b complex and analyzed using flow cytometry. (B) Mean fluorescence intensities of SIINFEKL-pulsed NP-Ab-K^b. The data are presented as the mean ± SD of five independent experiments. (C) NP-Ab-K^b was incubated with 0, 20, or 100 μM SIINFEKL for 18 h at 37°C. SIINFEKL-pulsed NP-Ab-K^b was stained using an mAb (Clone 25-D1.16) for the SIINFEKL-K^b complex and analyzed using flow cytometry. (D) Mean fluorescence intensities of SIINFEKL-pulsed NP-Ab-K^b. The data are presented as the mean ± SD of five independent experiments.
$^{**}p < 0.01$, $^{***}p<0.001$.

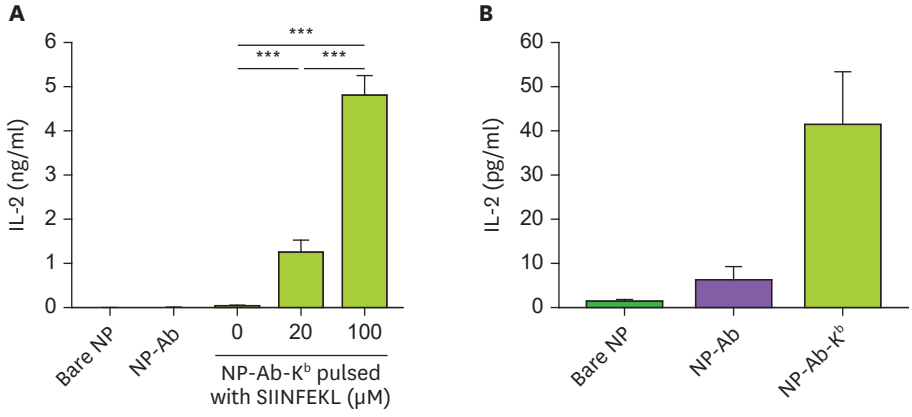

Figure 5. SIINFEKL-pulsed NP-Ab-K^b enhances MHC-I-restricted cross-presentation of SIINFEKL in DCs. DC2.4 cells (1×10^5 cells/well) were treated with PBS, bare NP, NP-Ab, or NP-Ab-K^b (1×10^8 particles/well) for 2 h. After washing and fixing, DCs were co-cultured with SIINFEKL-specific CD8OVA cells. The supernatants were harvested, and IL-2 production was measured by ELISA. The data are presented as the mean ± SD of five independent experiments.
$^{***}p<0.001$.

NP-Ab-K^b was injected and further increased to 2.5% when 100 μM SIINFEKL-pulsed NP-Ab-K^b was injected (**Fig. 6B**).

Seven days after the last immunization, SIINFEKL-specific CTL activity was assessed by an *in vivo* CTL assay using CFSE–labeled syngeneic target cells. Representative histograms are shown in **Fig. 6C**. The percent specific killing of SIINFEKL-pulsed target cells was 29.7%

https://doi.org/10.4110/in.2021.21.e44

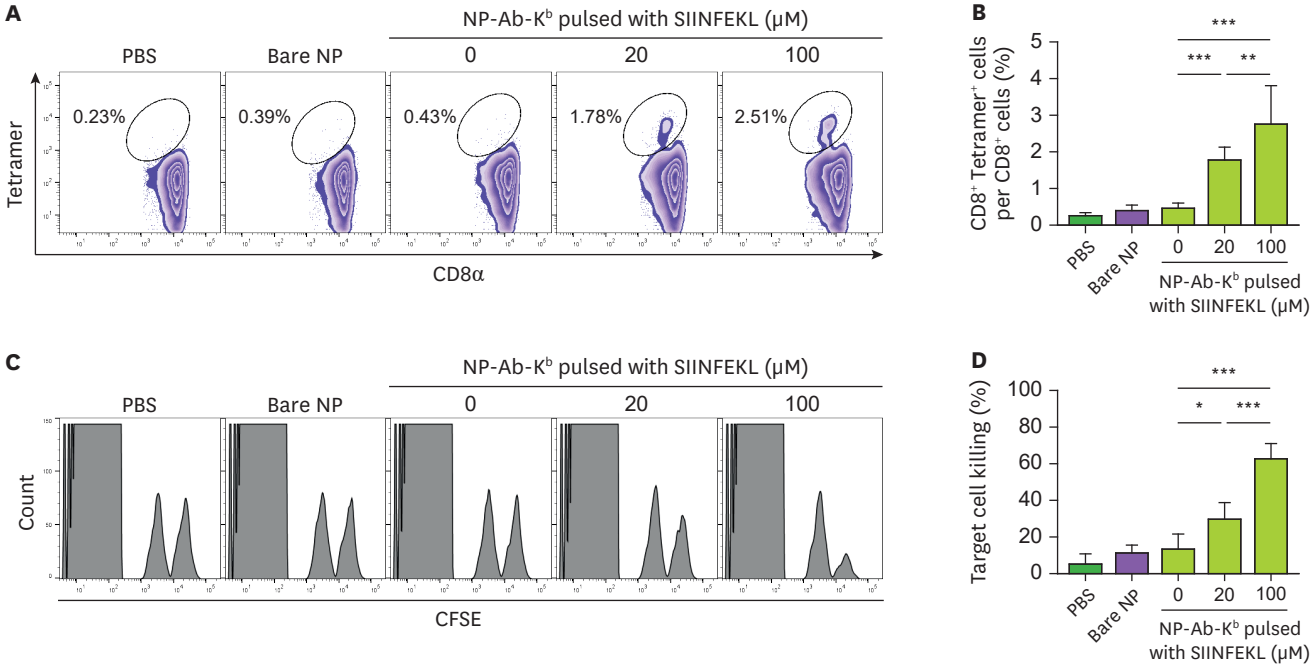

Figure 6. Injection of SIINFEKL-pulsed NP-Ab-K^b induces SIINFEKL-specific CTLs in normal mice. (A) PBS, bare NP, NP-Ab-K^b, 20 μM SIINFEKL-pulsed NP-Ab-K^b, or 100 μM SIINFEKL-pulsed NP-Ab-K^b (1×10^9 particles/mouse) were i.v. injected into C57BL/6 mice on days 0 and 7. On days 5 and 12, whole blood samples collected from the facial vein were stained with SIINFEKL-K^b tetramer and mouse CD8α mAb. (B) The frequency of SIINFEKL-specific CD8$^+$ T cells in each experimental group is shown. (C) SIINFEKL-specific cytotoxic activity was assessed using an *in vivo* CTL assay. CFSC-labeled target cells were i.v. injected into recipient mice on day 14, and the specific cytotoxicity was determined 18 h later by flow cytometric analysis of splenocytes. (D) The proportion of killed target cells in each experimental group is shown. The data are presented as the mean ± SD of at least two independent experiments (n=4–5 mice/group in each experiment). *p<0.05, **p<0.01, ***p<0.001.

when 20 μM SIINFEKL-pulsed NP-Ab-K^b was injected and further increased to 62.7% when 100 μM SIINFEKL-pulsed NP-Ab-K^b was injected (**Fig. 6D**).

Specific CTL-inducing activity of SIINFEKL-pulsed NP-Ab-K^b was also examined in tumor-bearing mice. Starting 2 days after s.c. inoculation with EG7.OVA tumor cells, the mice received three i.v. immunizations with SIINFEKL-pulsed NP-Ab-K^b, at 7-day intervals. Control mice received PBS or bare NP. Five days after the first immunization (post-priming) and the last immunization (post-boosting), peripheral blood was collected from each mouse by cheek bleeding, and SIINFEKL-specific CTLs were analyzed using SIINFEKL-loaded K^b tetramers. Immunization of tumor-bearing mice with SIINFEKL-pulsed NP-Ab-K^b potently induced SIINFEKL-specific CTLs (**Fig. 7A and C**). In mice injected with 100 μM SIINFEKL-pulsed NP-Ab-K^b, the relative frequency of SIINFEKL-specific CTLs among CD8$^+$ T cells was 1.8% in the post-priming group and further increased to 3.4% in the post-boosting group (**Fig. 7B and D**).

SIINFEKL-pulsed NP-Ab-K^b exerts potent anti-tumor activity in mice bearing EG7.OVA tumors

The anti-tumor therapeutic potential of SIINFEKL-pulsed NP-Ab-K^b was examined in EG7.OVA tumor-bearing mice. Starting 2 days after s.c. inoculation with EG7.OVA tumor cells, the mice received three i.v. injections of SIINFEKL-pulsed NP-Ab-K^b at 7-day intervals. Control mice received PBS or bare NP. Injection of mice with bare NP had no noticeable impact on tumor growth. In marked contrast, injection of mice with SIINFEKL-pulsed NP-Ab-K^b exerted potent anti-tumor activity (**Fig. 8**), resulting in almost complete tumor regression in mice injected with 100 μM SIINFEKL-pulsed NP-Ab-K^b.

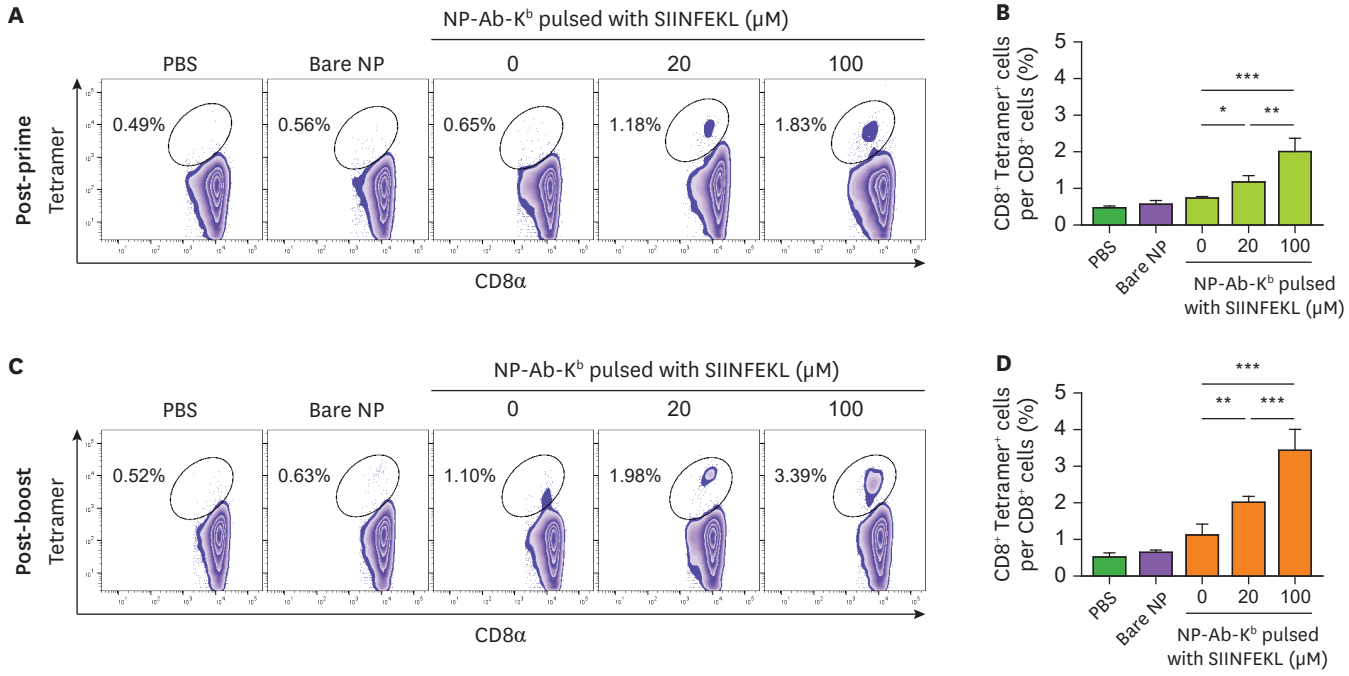

Figure 7. SIINFEKL-pulsed NP-Ab-K^b augments SIINFEKL-specific CD8$^+$ T cell expansion in EG7.OVA tumor-bearing mice. (A) C57BL/6 mice were s.c. inoculated with EG7.OVA tumor cells (3×10^5 cells/mouse) on day 0. PBS, bare NP, NP-Ab-K^b, 20 μM SIINFEKL-pulsed NP-Ab-K^b, or 100 μM SIINFEKL-pulsed NP-Ab-K^b (1×10^9 particles/mouse) were i.v. administered on days 2, 9, and 16. On day 7, whole blood samples were collected, stained with SIINFEKL-K^b tetramer and anti-mouse CD8α mAb (Clone KT15), and then analyzed using flow cytometry. (B) Dot plot showing relative frequency of SIINFEKL-specific CD8$^+$ T cells in each experimental group on day 7. (C-D) Dot plot showing relative frequency of SIINFEKL-specific CD8$^+$ T cells in each experimental group on day 21. The data are presented as the mean ± SD of at least two independent experiments (n=4–5 mice/group in each experiment).
*p<0.05, **p<0.01, ***p<0.001.

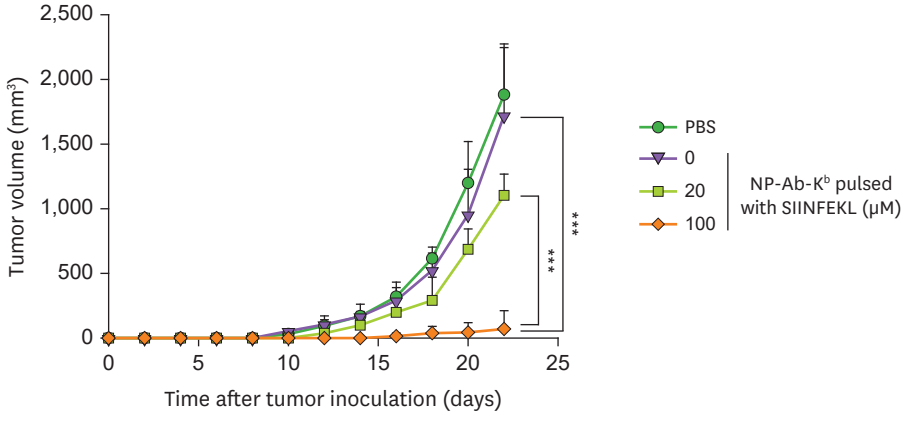

Figure 8. SIINFEKL-pulsed NP-Ab-K^b exerts potent anti-tumor activity in EG7.OVA tumor-bearing mice. C57BL/6 mice were s.c. inoculated with EG7.OVA tumor cells (3×10^5 cells/mouse) on day 0. PBS, bare NP, NP-Ab-K^b, 20 μM SIINFEKL-pulsed NP-Ab-K^b, or 100 μM SIINFEKL-pulsed NP-Ab-K^b (1×10^9 particles/mouse) were i.v. injected on days 2, 9, and 16. Tumor volume was measured every 2 days. The data are presented as the mean ± SD of at least two independent experiments (n=4–5 mice/group in each experiment). Significant differences between groups were evaluated by two-way ANOVA.
***p<0.001.

DISCUSSION

MHC-I-binding tumor peptide vaccines have several advantages over other immunotherapies, such as immune checkpoint inhibitors and CAR T cell therapy, because short peptides are

https://doi.org/10.4110/in.2021.21.e44

easy to synthesize and apply in clinical practice, are cost-effective, and are unlikely to induce Ag-induced anaphylaxis (8,12,26). However, most clinical studies using peptide vaccines have been disappointing. The challenges with therapeutic peptide vaccines include their poor immunogenicity and poor DC activation, binding to various cell types other than professional APCs, rapid degradation by tissue and serum peptidases, and an immunosuppressive tumor environment that prevents CTL induction (12,27). The vaccination strategy described here would provide a novel approach that circumvents most of these issues.

Notably, following *in vivo* administration, the tumor peptide-pulsed NP-Ab-K^b were efficiently phagocytosed by phagocytes including DCs, most probably due to opsonization by some of the Abs. Although NP-Ab was fabricated to facilitate 'tail-on' attachment of the Ab to the NP leaving the Ag-binding site (25), some of the Abs were conjugated via the Ag-binding site outside of the Fc region, allowing uptake by Fc-receptor-positive DCs. Prompt uptake of tumor peptide-pulsed NP-Ab-K^b by DCs is distinctively advantageous because tumor peptides can be delivered specifically to DCs. In addition, pre-binding of the peptides to K^b in the NP-Ab-K^b formulation prevents their binding to other K^b molecules expressed on non-APCs.

Phagocytosis of NPs can activate DC maturation and cytokine production (21,28). In line with this, we showed that uptake of NP-Ab-K^b by immature DCs led to their maturation accompanied by increased production of pro-inflammatory cytokines, such as IL-1β, IL-6, and TNF-α. In addition, following phagocytosis of tumor peptide-pulsed NP-Ab-K^b, DCs efficiently presented the tumor peptide in association with K^b molecules. It has been well-documented that cross-presentation of tumor peptides by professional APCs, particularly DCs, is critical for efficient generation of tumor peptide-specific CTLs (1,6,29-33). Direct presentation of tumor peptide-MHC-I complexes by tumor cells does not efficiently stimulate the CTLs, although it is crucial for tumor recognition by CTLs in the effector/cytolytic phase (34,35).

PLGA is a biocompatible and biodegradable polymer that is hydrolyzed to lactic and glycolic acids in the body and has been broadly used in pharmaceutical products as a drug carrier (36,37). PLGA-NPs are generally prepared using PVA as a particle stabilizer (38). In the present study, we substituted PVA with PEMA to generate carboxylated NPs. Next, anti-K^b mAb was covalently coupled to the NPs using a carbodiimide coupling reaction between the hydrophilic carboxyl side chains of NPs and the primary amine side chains of Abs (38,39). This NP-Ab was then incubated with solubilized membrane proteins isolated from a tumor mass (H-2^b) to produce NP-Ab-K^b. These NPs were stable for at least 9 days at 4°C with respect to particle size, ζ-potential, and the attachment of both the Ab and K^b molecules. The stability of NP-Ab-K^b is crucial for its clinical application, as it allows for advanced conjugation of NPs with anti-HLA-I Abs and storage at 4°C while the patient's tumor tissue is processed for isolation of HLA-I molecules. Once the patient's tumor mass is obtained, it takes just 2 days to prepare NP-Ab-HLA-I using solubilized membrane proteins isolated from the tumor and pulse it with the appropriate tumor peptides via peptide exchange reaction.

Injection of mice with SIINFEKL-pulsed NP-Ab-K^b exerted potent anti-tumor activity, resulting in almost complete tumor regression in mice implanted with EG7.OVA tumor cells. Because K^b molecules were isolated from EG7.OVA tumor cells, which are mouse thymoma EL4 cells stably transfected with the cDNA of OVA and thus express OVA epitopes in association with K^b, we expected that injection of mice with SIINFEKL-unpulsed NP-Ab-K^b also exerts anti-tumor activity. However, mice injected with SIINFEKL-unpulsed NP-Ab-K^b

did not exert discernable anti-tumor activity. This indicates that injection of NPs attached with endogenous SIINFEKL-K^b complexes are not enough to inhibit tumor growth.

This study was performed in only one tumor model using an immunogenic peptide as vaccine candidate. Future studies are warranted to test this vaccine strategy using more diverse peptide antigens in less immunogenic tumor models. Nevertheless, the peptide vaccination strategy described in this study may be applicable for other purposes, such as virus-specific CTL induction using a viral peptide, as long as MHC-I binding peptide epitopes are identified. We believe that this study lays the groundwork for efficient peptide-specific CTL induction *in vivo*.

ACKNOWLEDGEMENTS

This work was supported by the National Research Foundation of Korea (NRF) grant funded by the Korea government (NRF-2020R1A2C1009484, MRC-2017R1A5A2015541).

SUPPLEMENTARY MATERIALS

Supplementary Table 1

Summary of the characteristics of the NPs

Click here to view

Supplementary Table 2

Determination of the number of immobilized H-$2K^d$ molecules per NP

Click here to view

Supplementary Figure 1

Effects of NP-Ab-K^b on DC viability. (A) DC2.4 cells (5×10^4 cells/well) were incubated with bare NP or NP-Ab-K^b (6.25×10^6, 1.25×10^7, 2.5×10^7, or 5×10^7 particles/well) in 96-well plate for 24 h. The plate was washed twice with pre-warmed PBS, and 100 μL/well of complete culture medium without 2-ME was added. The cells were then incubated with 10 μL/well of WST-8 solution for 4 h. Absorbance was measured at 450 nm using a microplate reader. (B) BMDCs (5×10^5 cells/well) were incubated with bare NP or NP-Ab-K^b (6.25×10^7, 1.25×10^8, 2.5×10^8, or 5×10^8 particles/well) in a 96-well plate for 24 h. Cell viability was measured as described in (A).

Click here to view

Supplementary Figure 2

Determination of optimal dose of NP-Ab-K^b. C57BL/6 mice were i.v. immunized with PBS or SIINFEKL-pulsed NP-Ab-K^b (4×10^7, 2×10^8, or 1×10^9 particles/mouse) on days 0 and 7. On day 5 (A) and on day-12 (B), whole blood samples were collected, stained with SIINFEKL-K^b tetramer and anti-mouse CD8α mAb, and analyzed using flow cytometry. The dot plot shows the relative frequency of SIINFEKL-specific $CD8^+$ T cells in each experimental group. The data are presented as the mean ± SD of at least two independent experiments (n=5 mice/group in each experiment).

Click here to view

REFERENCES

1. Durgeau A, Virk Y, Corgnac S, Mami-Chouaib F. Recent advances in targeting CD8 T-cell immunity for more effective cancer immunotherapy. *Front Immunol* 2018;9:14.
PUBMED | CROSSREF
2. Malonis RJ, Lai JR, Vergnolle O. Peptide-based vaccines: current progress and future challenges. *Chem Rev* 2020;120:3210-3229.
PUBMED | CROSSREF
3. Wagner S, Mullins CS, Linnebacher M. Colorectal cancer vaccines: Tumor-associated antigens *vs* neoantigens. *World J Gastroenterol* 2018;24:5418-5432.
PUBMED | CROSSREF
4. Tanna JG, Ulrey R, Williams KM, Hanley PJ. Critical testing and parameters for consideration when manufacturing and evaluating tumor-associated antigen-specific T cells. *Cytotherapy* 2019;21:278-288.
PUBMED | CROSSREF
5. Schietinger A, Philip M, Schreiber H. Specificity in cancer immunotherapy. *Semin Immunol* 2008;20:276-285.
PUBMED | CROSSREF
6. Minati R, Perreault C, Thibault P. A roadmap toward the definition of actionable tumor-specific antigens. *Front Immunol* 2020;11:583287.
PUBMED | CROSSREF
7. Olsen LR, Campos B, Barnkob MS, Winther O, Brusic V, Andersen MH. Bioinformatics for cancer immunotherapy target discovery. *Cancer Immunol Immunother* 2014;63:1235-1249.
PUBMED | CROSSREF
8. Pallerla S, Abdul AU, Comeau J, Jois S. Cancer vaccines, treatment of the future: With emphasis on her2-positive breast cancer. *Int J Mol Sci* 2021;22:22.
PUBMED | CROSSREF
9. Cho HI, Barrios K, Lee YR, Linowski AK, Celis E. BiVax: a peptide/poly-IC subunit vaccine that mimics an acute infection elicits vast and effective anti-tumor CD8 T-cell responses. *Cancer Immunol Immunother* 2013;62:787-799.
PUBMED | CROSSREF
10. Barrios K, Celis E. TriVax-HPV: an improved peptide-based therapeutic vaccination strategy against human papillomavirus-induced cancers. *Cancer Immunol Immunother* 2012;61:1307-1317.
PUBMED | CROSSREF
11. Kumai T, Kobayashi H, Harabuchi Y, Celis E. Peptide vaccines in cancer-old concept revisited. *Curr Opin Immunol* 2017;45:1-7.
PUBMED | CROSSREF
12. Kumai T, Fan A, Harabuchi Y, Celis E. Cancer immunotherapy: moving forward with peptide T cell vaccines. *Curr Opin Immunol* 2017;47:57-63.
PUBMED | CROSSREF
13. Ahonen CL, Doxsee CL, McGurran SM, Riter TR, Wade WF, Barth RJ, Vasilakos JP, Noelle RJ, Kedl RM. Combined TLR and CD40 triggering induces potent CD8+ T cell expansion with variable dependence on type I IFN. *J Exp Med* 2004;199:775-784.
PUBMED | CROSSREF
14. He X, Abrams SI, Lovell JF. Peptide delivery systems for cancer vaccines. *Adv Ther* 2018;1:1800060.
CROSSREF
15. Khong H, Overwijk WW. Adjuvants for peptide-based cancer vaccines. *J Immunother Cancer* 2016;4:56.
PUBMED | CROSSREF
16. Xia F, Qian CR, Xun Z, Hamon Y, Sartre AM, Formisano A, Mailfert S, Phelipot MC, Billaudeau C, Jaeger S, et al. TCR and CD28 concomitant stimulation elicits a distinctive calcium response in naive T cells. *Front Immunol* 2018;9:2864.
PUBMED | CROSSREF
17. Davis SJ, Ikemizu S, Evans EJ, Fugger L, Bakker TR, van der Merwe PA. The nature of molecular recognition by T cells. *Nat Immunol* 2003;4:217-224.
PUBMED | CROSSREF
18. Raskov H, Orhan A, Christensen JP, Gögenur I. Cytotoxic CD8^{+} T cells in cancer and cancer immunotherapy. *Br J Cancer* 2021;124:359-367.
PUBMED | CROSSREF
19. Jeong S, Park SH. Co-stimulatory receptors in cancers and their implications for cancer immunotherapy. *Immune Netw* 2020;20:e3.
PUBMED | CROSSREF

20. Im SJ, Ha SJ. Re-defining T-cell exhaustion: subset, function, and regulation. *Immune Netw* 2020;20:e2.
PUBMED | CROSSREF
21. Jung HH, Kim SH, Moon JH, Jeong SU, Jang S, Park CS, Lee CK. Polymeric nanoparticles containing both antigen and vitamin D3 induce antigen-specific immune suppression. *Immune Netw* 2019;19:e19.
PUBMED | CROSSREF
22. Lee YH, Lee YR, Kim KH, Im SA, Song S, Lee MK, Kim Y, Hong JT, Kim K, Lee CK. Baccatin III, a synthetic precursor of taxol, enhances MHC-restricted antigen presentation in dendritic cells. *Int Immunopharmacol* 2011;11:985-991.
PUBMED | CROSSREF
23. Oyewumi MO, Kumar A, Cui Z. Nano-microparticles as immune adjuvants: correlating particle sizes and the resultant immune responses. *Expert Rev Vaccines* 2010;9:1095-1107.
PUBMED | CROSSREF
24. Sadat SM, Jahan ST, Haddadi A. Effects of size and surface charge of polymeric nanoparticles on *in vitro* and *in vivo* applications. *J Biomater Nanobiotechnol* 2016;7:91-108.
CROSSREF
25. Lou D, Ji L, Fan L, Ji Y, Gu N, Zhang Y. Antibody-oriented strategy and mechanism for the preparation of fluorescent nanoprobes for fast and sensitive immunodetection. *Langmuir* 2019;35:4860-4867.
PUBMED | CROSSREF
26. Slingluff CL Jr. The present and future of peptide vaccines for cancer: single or multiple, long or short, alone or in combination? *Cancer J* 2011;17:343-350.
PUBMED | CROSSREF
27. Dellacherie MO, Li AW, Lu BY, Mooney DJ. Covalent conjugation of peptide antigen to mesoporous silica rods to enhance cellular responses. *Bioconjug Chem* 2018;29:733-741.
PUBMED | CROSSREF
28. Foged C, Brodin B, Frokjaer S, Sundblad A. Particle size and surface charge affect particle uptake by human dendritic cells in an in vitro model. *Int J Pharm* 2005;298:315-322.
PUBMED | CROSSREF
29. Kurts C, Robinson BW, Knolle PA. Cross-priming in health and disease. *Nat Rev Immunol* 2010;10:403-414.
PUBMED | CROSSREF
30. Chen L, Fabian KL, Taylor JL, Storkus WJ. Therapeutic use of dendritic cells to promote the extranodal priming of anti-tumor immunity. *Front Immunol* 2013;4:388.
PUBMED | CROSSREF
31. Schiavoni G, Mattei F, Gabriele L. Type I interferons as stimulators of DC-mediated cross-priming: impact on anti-tumor response. *Front Immunol* 2013;4:483.
PUBMED | CROSSREF
32. Rundqvist H, Veliça P, Barbieri L, Gameiro PA, Bargiela D, Gojkovic M, Mijwel S, Reitzner SM, Wulliman D, Ahlstedt E, et al. Cytotoxic T-cells mediate exercise-induced reductions in tumor growth. *eLife* 2020;9:9.
PUBMED | CROSSREF
33. Gong Y, Suzuki T, Kozono H, Kubo M, Nakano N. Tumor-infiltrating CD62L+PD-1-CD8 T cells retain proliferative potential via Bcl6 expression and replenish effector T cells within the tumor. *PLoS One* 2020;15:e0237646.
PUBMED | CROSSREF
34. Huang AY, Golumbek P, Ahmadzadeh M, Jaffee E, Pardoll D, Levitsky H. Role of bone marrow-derived cells in presenting MHC class I-restricted tumor antigens. *Science* 1994;264:961-965.
PUBMED | CROSSREF
35. Arina A, Tirapu I, Alfaro C, Rodríguez-Calvillo M, Mazzolini G, Inogés S, López A, Feijoo E, Bendandi M, Melero I. Clinical implications of antigen transfer mechanisms from malignant to dendritic cells. exploiting cross-priming. *Exp Hematol* 2002;30:1355-1364.
PUBMED | CROSSREF
36. Wang Q, Wang J, Lu Q, Detamore MS, Berkland C. Injectable PLGA based colloidal gels for zero-order dexamethasone release in cranial defects. *Biomaterials* 2010;31:4980-4986.
PUBMED | CROSSREF
37. Hamdy S, Haddadi A, Hung RW, Lavasanifar A. Targeting dendritic cells with nano-particulate PLGA cancer vaccine formulations. *Adv Drug Deliv Rev* 2011;63:943-955.
PUBMED | CROSSREF
38. Keegan ME, Royce SM, Fahmy T, Saltzman WM. *In vitro* evaluation of biodegradable microspheres with surface-bound ligands. *J Control Release* 2006;110:574-580.
PUBMED | CROSSREF
39. Cao J, Choi JS, Oshi MA, Lee J, Hasan N, Kim J, Yoo JW. Development of PLGA micro- and nanorods with high capacity of surface ligand conjugation for enhanced targeted delivery. *Asian J Pharm Sci* 2019;14:86-94.
PUBMED | CROSSREF